Full length article

Soft novel form of white-etching matter and ductile failure of carbide-free bainitic steels under rolling contact stresses

W. Solano-Alvarez [a, *], E.J. Pickering [b], M.J. Peet [a], K.L. Moore [b], J. Jaiswal [c], A. Bevan [c], H.K.D.H. Bhadeshia [a]

[a] Department of Materials Science and Metallurgy, University of Cambridge, UK
[b] School of Materials, University of Manchester, UK
[c] Institute of Railway Research, University of Huddersfield, UK

ABSTRACT

There has been a great deal of work on the formation of hard white-etching regions in conventional bearing steels such as 1C-1.5Cr wt% when subjected repeatedly to rolling contact stresses. The regions are a consequence of localised mechanical attrition across microcrack faces and mixing, which refine the local structure and force cementite to dissolve. This white-etching matter is often associated with brittle phenomena because the hardness can exceed 1100 HV. In contrast, carbide-free mixtures of bainitic ferrite and retained austenite when subjected to the same loading have been unexpectedly found not to develop the characteristic patches of hard material and to show instead signs of ductility in the attrited regions. The work presented here shows that the white-etching areas that develop in carbide-free bainite are *softer* than their surroundings, whether they are in hard nanostructured bainite destined for bearing applications or when the steel is designed for the manufacture of rails. Advanced characterisation tools were used for the first time to understand carbon redistribution during its formation. The deep interest about soft white-etching matter originates from the idea that it could lead to the reduction in premature failure of wind turbine gearbox bearings and white-etching layer grinding of rails.

© 2016 Acta Materialia Inc. Published by Elsevier Ltd. This is an open access article under the CC BY license (http://creativecommons.org/licenses/by/4.0/).

1. Introduction

Previous studies have highlighted the potential of nano-structured bainite, which consists of fine plates of bainitic ferrite in a matrix of stable austenite, as a bearing steel due to its hardness (600–670 HV), toughness (30–40 MPa m$^{1/2}$), and rolling-sliding wear resistance [1–5]. The first study on this topic suggested that the predominant damage mechanism when the bainite is subjected to rolling contact fatigue (RCF) is ductile void formation at interfaces [6]. The voids then grow and coalesce into larger entities that lead ultimately to fracture.

This is in contrast to the well-studied mechanism of brittle crack initiation at inclusions in standard quenched and tempered 1C-1.5Cr wt% bearing-steels. In these steels, the material in the vicinity of the cracks changes into the so-called white-etching region that is a consequence of severe localised mechanical mixing of the microstructural constituents [7]. Due to the brittleness of these

alloys [8] and the hardness of the white deformed regions, these white-etching cracks (WECs), or butterfly cracks[1] eventually link up into larger networks that lead to spalling [11]. This mechanism is referred to as "white structure flaking" [10,14]. It is important to emphasise that the white-etching matter (WEM) that causes the greatest damage is that which is harder than the surrounding matrix, the additional hardness having its origin in the state of deformation and because cementite is taken into solution by mechanical alloying [9,15,16].

In a recent critical assessment on the topic, it was concluded that three ways to ameliorate the occurrence of damaging hard white-etching matter in conventional steels are: an increase in

---

* Corresponding author.
  E-mail address: ws298@cam.ac.uk (W. Solano-Alvarez).

[1] White-etching cracks can refer to subsurface inclusion-initiated cracks that propagate hundreds of micrometers long and later develop white-etching regions around the faces normal to the compressive axis of the contact stress, whereas butterflies refer to subsurface defect initiated short cracks, tens of micrometers long, that later develop white-etching regions around them giving them the appearance of white-winged butterflies [9–11]. However, we note that there exists also evidence for contact surface initiated cracks that lead to white-etching crack arrays, and there may well be other mechanisms possible [12,13].

toughness to avoid cracks from localising deformation; the trapping or prevention of diffusible hydrogen, and the removal of carbides from the microstructure [9]. In light of this, we report a more detailed study of carbide-free nanostructured bainite under rolling contact fatigue, that has revealed scarce examples of butterflies with associated white-etching matter, and carbide-free bainite from a serviced rail that revealed abundant white-etching matter around rolling contact fatigue cracks (also called white-etching cracks). Both white-etching matter manifestations are characterised and shown to have similar properties between them, but quite different from those associated with conventional carbide-containing steels in terms of hardness and damage mechanisms. The softness of the white-etching matter, despite being a region of localised deformation, could be a game changer in the development of carbide-free steels to resist white-structure flaking, which causes the premature failure of large wind turbine gearbox bearings at only 10% of their expected life [14]. Likewise, soft white-etching layers on the surface of rails could eliminate the need for vehicle mounted grinding, since these could easily be worn away by regular traffic.

2. Experimental methods

2.1. Bearing steel

2.1.1. Material and sample preparation

The alloy used for rolling contact fatigue samples was produced by *Tata Steel* UK as an ingot subjected to electroslag remelting, vacuum arc remelting, annealing, cold straightening, smooth turning, and rolling to a 180 mm in diameter shaft. The chemical composition is described in Table 1.

Cylindrical samples, 9.53 mm in diameter and 120 mm in length, were cut out from the edges of the shaft along its longitudinal direction using a band saw, ground manually to a cylindrical shape, turned, and polished to a 1 μm finish to avoid surface initiated damage during rolling contact.

2.1.2. Heat treatment

Before heat treatment, the samples were wrapped tightly in four layers of steel foil to avoid decarburisation. They were then austenitised in a *Carbolite* RWF1200 box furnace at 930 °C for 30 min, cooled in air to 250 °C, which took approximately 6 min, introduced into an oven for isothermal heat treatment at 200 °C for 10 days, and cooled in air. The heat treatment was simulated using *MTDATA* coupled with the *TCFE* database and *MATCALC* [17,18]. In order to corroborate the efficacy of the heat treatment in generating nanostructured bainite, samples were analysed using microscopy and Vickers hardness measurements.

2.1.3. Rolling contact fatigue testing

The samples were then tested under lubricated rolling contact fatigue, without hydrogen charging or transient conditions to accelerate damage evolution, using a *Delta Research Corporation BR-4* Ball-Rod test rig at room temperature, at a rotational speed of 3600 rpm (the design of the test rig allows ~2.4 stress cycles per revolution), and a Hertzian pressure of 3.5 GPa. More detail on the mechanics of the testing rig or test specifications can be found in Ref. [6]. Specimens were stopped when the vibration thresholds were exceeded, as measured by an accelerometer due to unintended lubrication failure. In the current study, the specimens that failed after 41 h (2.1×10^7 cycles) and 948 h (4.9×10^8 cycles) were analysed.

2.2. Rail steel

2.2.1. Field samples

Although the usages of steel grades used in railway networks is dominated by pearlitic grades, the industry has undertaken trials with several steel compositions covering a range of bainitic microstructures. One such grade is a low carbon carbide-free steel manufactured by *British Steel* France with composition stated in Table 2, tensile strength of 1.23 GPa, and 15% elongation. The steel composition has been deployed in trial sites in several European networks and is the approved grade for movable frog points for the French network. The aspect of particular interest with the research reported in this paper stems from the much lower carbon content and the virtual absence of carbides in the microstructure of this grade. A 300 mm long sample taken from of a trial rail exhibiting isolated RCF cracks at the gauge corner of the running surface became available and presented an opportunity to examine the microstructural features to compare with those from specialist RCF tests undertaken on higher carbon nanobainitic steel. Establishing the factors that contributed to the formation of the observed cracks is beyond the scope of the work presented here since it would require further microscopy and detailed information of the rail-wheel contact conditions. However, it is suspected that the cracks could be the result of unusual track conditions created by rough grinding.

The section analysed was located within a 1000 m radius curve, which experienced 120 MGT (Million Gross Tonnes) with axle loads up to 22.5 tonnes per axle. The track was ground every year by a mounted grinding vehicle using ~25 MGT with the purpose of eliminating nascent surface cracks. The rail head was cut and cooled in liquid nitrogen to reveal the crack face by breaking it open.

2.3. Microstructural characterisation

The RCF tested samples, sectioned along the radial cross section as described in Ref. [19], and the rail sample, sectioned along the length just under the gauge corner, were mounted in bakelite, ground, polished to 0.25 μm, etched in 2% nital, and characterised using a *FEI Nova NanoSEM* (scanning electron microscope) equipped with a *Bruker XFlash 6—100* energy dispersive X-ray spectrometer (EDX) and a *Bruker* electron backscatter diffraction (EBSD) camera. Specific regions of white-etching butterfly wings in each of the two nanobainitic RCF samples as well as the white-etching matter around the crack in the rail sample were extracted using a focused ion beam (FIB) in a *FEI Helios Nanolab* dual beam field emission SEM and observed with a *JEOL 200CX* transmission

Table 2
Chemical composition of serviced rail, wt%.

C	Mn	Si	Cr	Mo	P	S	B
0.33	1.52	1.25	0.527	0.17	0.019	0.014	3 ppmw

Table 1
Chemical composition of rolling contact fatigue samples, wt%.

C	Mn	S	P	Si	Al	Cu	Cr	Ni	Mo	V	Nb	Ti	B
0.8	2.03	0.006	0.006	1.51	0.057	0.03	0.22	1.05	0.377	0.004	0.007	0.019	0.0007

electron microscope (TEM) or a *FEI Tecnai Osiris 80-200*, which was used for scanning transmission electron microscopy (STEM) bright field (BF) and high-angle annular dark field (HAADF) imaging with an accelerating voltage of 200 kV. In order to compare the carbon concentration of different regions in the extracted lamellae of the nanobainitic butterflies, electron energy loss spectroscopy (EELS) was performed using a *Gatan Enfinium ER 977* spectrometer in the *Tecnai Osiris* [20,21]. Carbon distribution and mapping of other light elements around the crack in the rail sample was achieved using nanoscale secondary ion mass spectroscopy (NanoSIMS). A *Cameca NanoSIMS 50L* was used with a 16 keV Cs^+ primary ion beam with a current of 0.8–2.7 pA and aligned to detect $^{12}C^-$, $^{16}O^-$, $^{12}C^{14}N^-$, $^{31}P^-$, $^{32}S^-$ and $^{11}B^{16}O^{2-}$. Cs^+ ions were implanted into the surface prior to imaging to achieve a dose of 1×10^{17} ions cm^{-2} to ensure that each imaged area was at steady state and to remove any native oxide.

Phase volume fractions using X-ray diffraction (XRD) in the RCF nanobainite samples are reported in the initial study [6]. After microscopy, Vickers microhardness of the white-etching butterfly wings, white-etching cracks, and the bulk material around cracks without white-etching matter was measured with a *Qness* hardness machine using a dwell time of 10 s and a load of 0.01 kg for the RCF samples or 0.02 kg for the rail sample due to the difference in size of the white-etching regions. Three butterfly wings were measured in the 948 h sample (29 indentations), two wings in the 41 h sample (10 indentations), and 25 indentations on the white-etching matter around the crack of the rail sample. The matrix macrohardness of the nanostructured bainite and rail bainite were also measured by performing 10 indentations with a 30 kg load. A summary of the microstructural characterisation tools used is presented in Fig. 1.

3. Results and discussion

The Vickers microhardness results are summarised in Table 3. In both nanostructured RCF samples, the WEM is 9–10% *softer* than the matrix, whereas in the bainitic rail, the WEM was 48% softer. The explanation for such softness will be discussed later, after the results of the microscopy are presented. To allow for the possibility of crack proximity affecting the hardness measurements, the bulk material was indented in the vicinity of WEM-free voids and cracks (Fig. 4b). It is worth mentioning that a similar approach was followed when determining the microhardness of the WEM formed around cracks in martensitic 1C-1.5Cr steel where the WEM turned out to be 10% harder than the matrix, corroborating therefore the validity of the results found here and eliminating the doubt that the softness is simply caused by crack proximity [19]. It is noted that due to the small load (0.01 kg) used for the indentations in the nanobainitic RCF samples, the hardness is higher than the macroscopic value of 632 ± 2 HV30 for the matrix, but the relative trends should be correct. The higher load (0.02 kg) used with the bainitic rail reveals a closer proximity to the macroscopic value of the matrix, which is 390 ± 2 HV30.

Carbide-free nanostructured bainite for bearings	Carbide-free bainite for rails
MATCALC/MTDATA Hardness XRD SEM-EDX EBSD FIB-TEM/STEM (BF+HAADF) EELS	Hardness SEM FIB-TEM nanoSIMS

Fig. 1. Characterisation techniques used.

Table 3
Vickers microhardness average values and standard error of the white-etching matter in butterflies/around cracks and bulk material performed with a 0.01 kg load in case of the nanobainitic RCF samples and 0.02 kg for the bainitic rail.

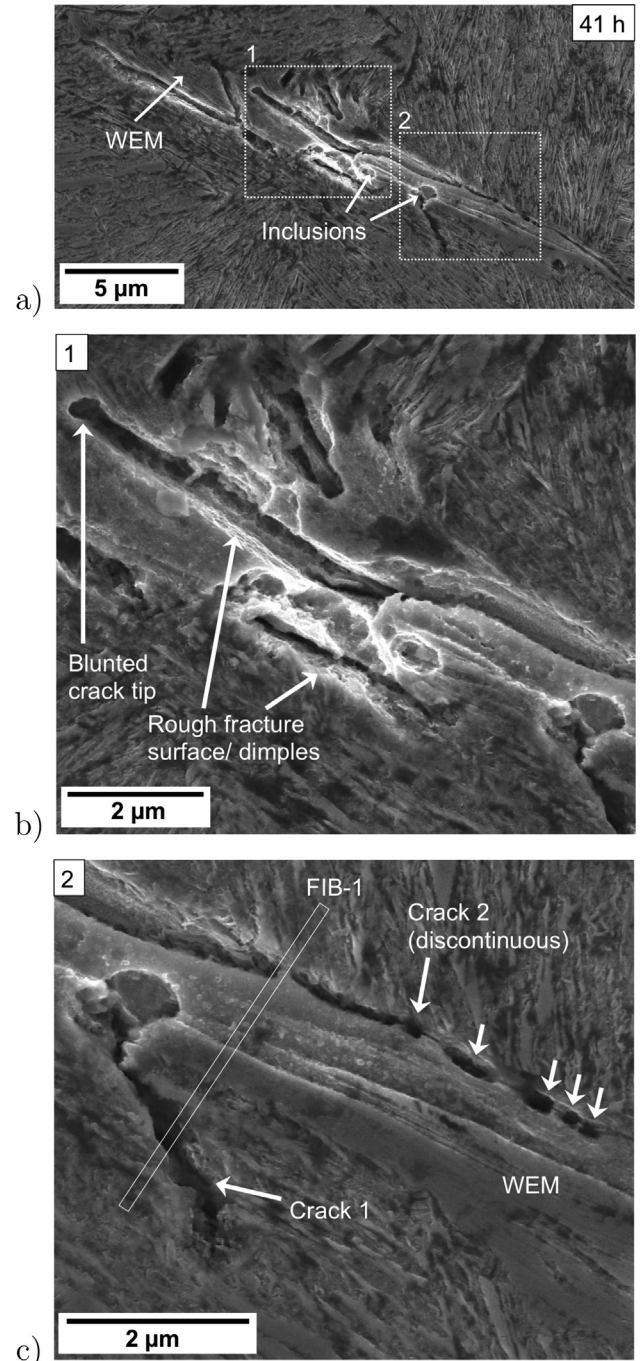| Sample	WEM	Bulk
41 h	752 ± 14	833 ± 7
948 h	766 ± 10	839 ± 7
Rail	214 ± 13	409 ± 8

Fig. 2. Secondary electron SEM image of a) butterfly studied in the sample that ran for 41 h with b) detail of cracks in area 1 and c) location of the extracted lamella (FIB-1) in area 2.

The annotated images of the butterflies studied in the nanostructured bainite after rolling contact fatigue testing are presented in Figs. 2 and 3. In the butterfly present in the sample that lasted 41 h, a few different inclusions were observed but none of them seemed to be the origin of the butterfly cracks. It is likely that the main inclusion was either ground away during preparation or located further inside the material. Nonetheless, suspected WEM areas due to their distinct topography were still found along those cracks and a region was selected for FIB extraction (FIB-1). Despite etching artefacts, the shape of the first butterfly in the 948 h sample (Fig. 3a) is more conventional with just two cracks at opposite sides of the main inclusion. However, the total crack length and amount of WEM is similar to the one in the 41 h sample, possibly suggesting no progressive damage evolution due to the presence of WEM, a fact that could be attributed to its softness with respect to the matrix.

In conventional quenched and tempered bearing steels, WEM has been found to be harder than the surrounding matrix, owing to the dissolution of carbides and the resulting carbon supersaturation of the nanostructured ferrite [9,15,16]. Once WEM is formed through the rubbing of cracks [19], its high hardness is then thought to enhance crack propagation and further WEM formation in a concomitant process [14,15,22]. Here, however, we have observed WEM that is softer than the matrix, which by the same reasoning, would not be expected to enhance crack propagation. It should be noted that a decrease in stress concentration with increasing distance from the initiation site could also play a role in limiting crack length since further growth is said to require a transition from Mode I to Mode II/III shear loading as the normal stress acts as a crack closing load [23–25]. However, it is still expected that the formation of soft WEM would lead to a greater resistance to crack propagation.
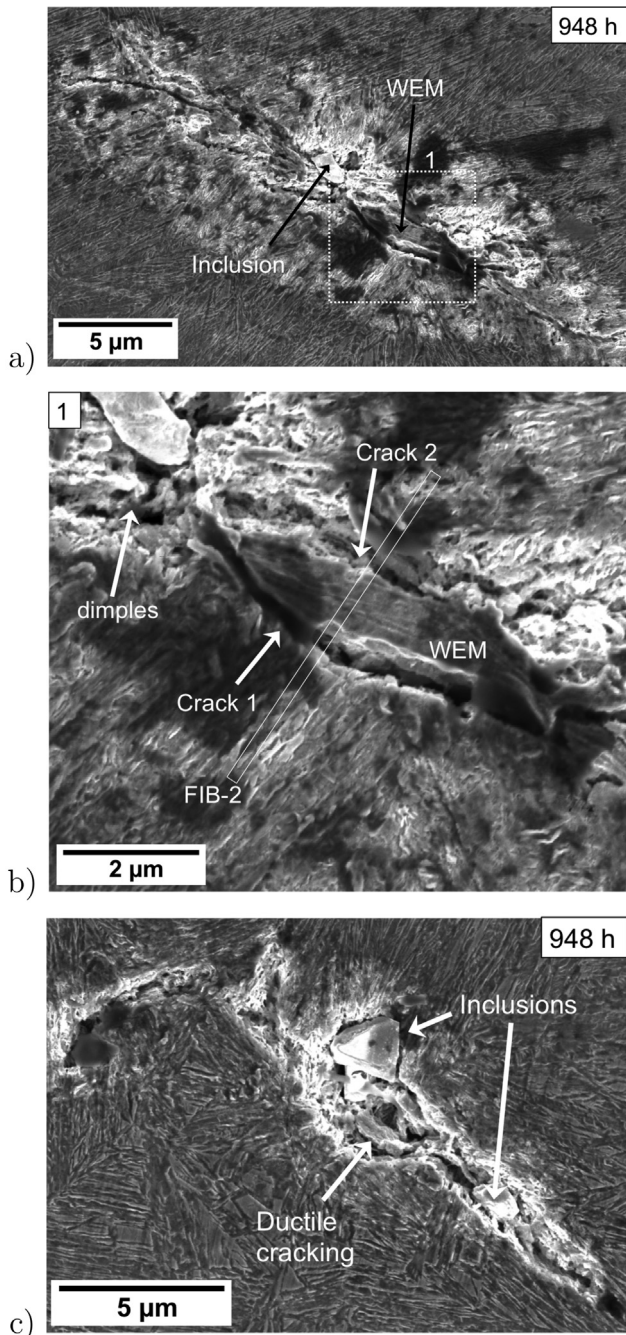

Fig. 3. Secondary electron SEM image of two butterflies (a and c) found in the sample that ran for 948 h with b) location of the extracted lamella (FIB-2) in area 1.
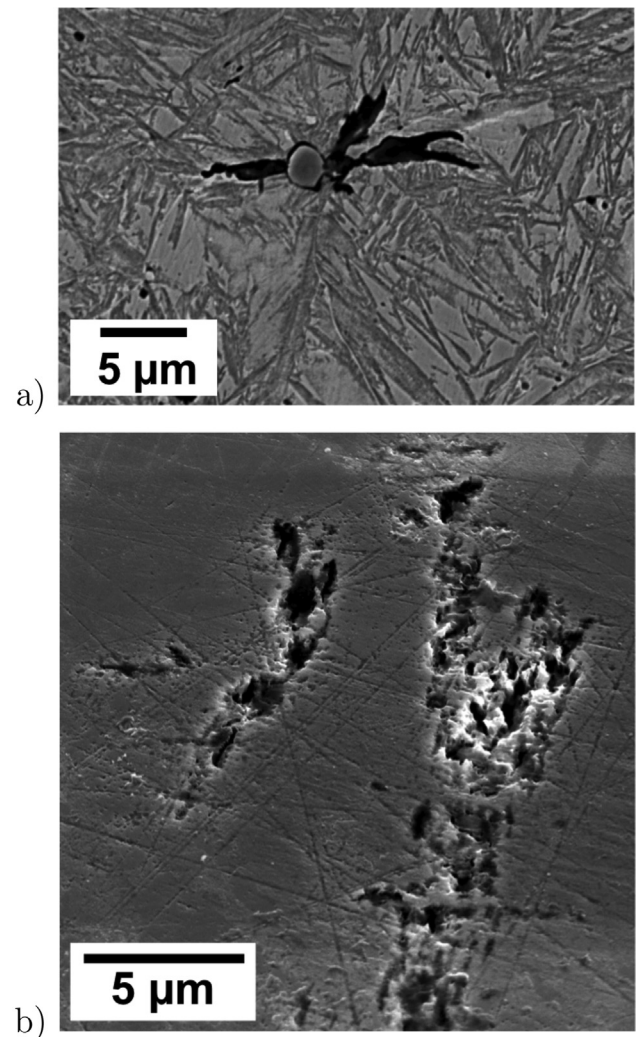

Fig. 4. Secondary electron SEM images of a) brittle butterfly cracks with sharp tips in a martensitic 1C-1.5Cr steel tested at 3.5 GPa using the same rod-ball RCF machine and b) void-coalesced crack in the nanostructured bainite sample that clocked 948 h showing ductile void formation and a lack of surrounding WEM. The sample was tilted 52° with respect to the electron beam to distinguish more clearly the misshapen appearance of the damaged region.

The chemical compositions of all five inclusions marked in Figs. 2 and 3 consisted of Mg, Al, and O, as measured using EDX. Despite electroslag and vacuum arc remelting, inclusions of similar composition were found to be the source of fatigue cracks in a Co-containing air melt nanostructured bainite steel [26] and in a medium-C low-Ni variety [3]. It is also worth mentioning that the depths relative to the contact surface of the butterflies presented here (126 μm for the 41 h sample and 101 and 114 μm respectively for the 948 h sample) are in agreement with the calculated maximum subsurface orthogonal shear stress of 99 μm for a 3D frictionless elastic Hertzian contact scenario, rather than the unidirectional shear stress that has a maximum at 190 μm below the surface [6,27].

Despite the fact that *MATCALC* confirmed the possibility of 0.1 wt % pro-eutectoid cementite forming at 730 °C during air cooling (using 2 °C s^{-1}) from the austenitisation temperature to the austempering temperature, as well as incomplete solubility of Nb and V carbides at 930 °C using *MTDATA*, no metallographic evidence of any of these was found confirming the carbide-free nature of the alloy and eliminating the possibility of carbides being the source of the observed white-etching matter butterflies [25].

A few important aspects to note about the cracks formed around inclusions are that they are discontinuous (Fig. 2c), have a misshapen appearance (Fig. 3c), possess dimples at the fracture surface, and have blunted tips (Fig. 2b). These features indicate ductile failure, unlike the well-documented brittle cracking at inclusions in conventional 1C-1.5Cr steels (Fig. 4a) [14]. The observations are consistent with the ductile void formation failure mechanism of the nanostructured bainitic matrix under rolling contact fatigue [6]. However, it is important to mention that only the ductile cracks nucleated from inclusions (butterflies) generated white-etching matter around them and not the void-coalesced cracks that appear in the subsurface of the matrix (Fig. 4b). This is probably because the latter cracks are spread over larger regions so that the level of localised plastic deformation is less; the earlier study (Fig. 7c in Ref. [6]) showed a rim below the contact surface where voids were distributed uniformly all along the entire circumference.

EBSD patterns performed at two different locations within the depth of maximum subsurface orthogonal shear stress in the 948 h sample after polishing with colloidal silica are presented in Fig. 5. The resolution is naturally limited by the technique (not sufficient to assess nanostructural changes) but the images nevertheless show that there is no major disruption of the structure in spite of the voiding damage mechanism caused by the subsurface shear stresses due to prolonged rolling contact. Likewise, the phase maps shown in Fig. 5c and d are evidence of the stability of the larger carbon-enriched retained austenite regions (which should be less mechanically stable than the films [28,29]) and agree with X-ray diffraction data [6] that revealed a fraction 0.21 ± 0.01 of retained austenite persisting after RCF. Both the integrity of the nanostructure and stability of the retained austenite (due to its volumetric expansion in the event of martensitic transformation) are important factors when considering a steel for bearing
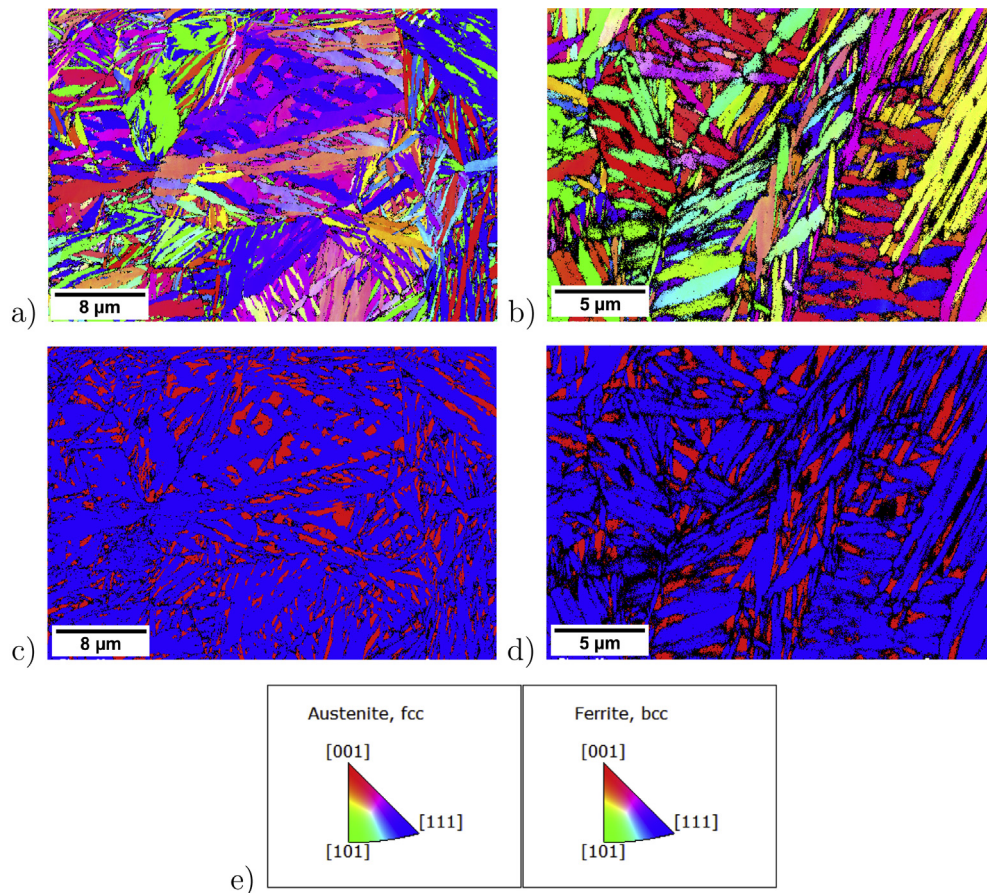

Fig. 5. EBSD maps of two different regions: region 1 (a and c) acquired with a step size of 67 nm, a voltage of 20 kV and a working distance of 15 mm, and region 2 (b and d) using a step size of 42 nm, a voltage of 20 kV and a working distance of 14.9 mm (a and b) are standard inverse pole figure maps (key in e) and (c and d) show phase maps with bainitic ferrite coloured blue and retrained austenite in red. (For interpretation of the references to colour in this figure legend, the reader is referred to the web version of this article.)

performance given the need of dimensional stability that arises from the reduced clearance of the cage and raceways, as well as the interference fit of the inner ring with the supporting shaft [7,30].

The TEM bright field images and associated electron diffraction patterns of the extracted lamellae are presented in Figs. 6 and 7. Due to contrast artefacts in Fig. 6, the borders of the lamella in the low magnification frame as well as the suspected WEM regions are outlined with a black solid and dashed white line respectively. Cracks are marked to show correspondence to the SEM images. Despite the already nanostructured pattern of the bainitic ferrite matrix, the suspected WEM regions show a very distinct dotted morphology consisting of fine equiaxed ferrite grains, 20—40 nm in diameter, and a characteristic ring-like powder diffraction pattern due to its fine scale, which confirms they are indeed white-etching matter. In the case of the 948 h sample, the electron diffraction pattern indicates the development of a preferred crystallographic orientation or texture of the nanosized ferritic grains. It is worth mentioning that although the matrix does show progressive microstructural degradation after 948 h of RCF, it is not related to the presence of white-etching matter since the same degradation was observed in the WEM-free void coalesced cracks in the original study [6].

In order to study the behaviour of carbon redistribution, electron energy loss spectroscopy (EELS) was performed, for the first time in the context of butterflies and white-etching cracks, in two different regions of lamella FIB-2 (948 h sample) marked with yellow solid line rectangles in the low magnification image (Fig. 7). The resulting greyscale maps, where black pixels represent the maximum carbon content detected, are superimposed on their respective scanned regions in the STEM image. The results (EELS-1) indicate that there is slightly less carbon dissolved in the WEM than in the matrix, which is consistent with the 10% lower hardness of the white deformed region. Since EELS is a thickness sensitive measurement, the reduced signal intensity of the WEM could nevertheless represent simply a thicker region than the matrix due

to differences in ion milling rates. In order to separate out the influence of thickness from the measurements, a vertical scan (EELS-2) was run knowing that the focused ion beam process leads to samples which are thicker at the bottom. The result from the vertical scan still shows a lower amount of carbon in the WEM compared to the thicker matrix bottom, giving more confidence on the relative qualitative accuracy of this technique. Previous studies have proven the usefulness of EELS in understanding carbon diffusion, for example, after cementite decomposition during the formation of hard white-etching layers on the surfaces of pearlitic rail steels [31].

3.1. Carbide-free bainitic rail

Macroscopic images of the serviced carbide-free bainitic rail are shown in Fig. 8. Annotated SEM images of the crack studied are shown in Fig. 9. The crack shown in Fig. 9a is a minor branched crack located ~500 μm deep under the gauge corner along the length of the rail, although the true depth is most likely to be around 5 mm due to the loss of rail profile caused by wear and grinding operations (Fig. 8a) [32]. The abrupt upper edge of the steel in image Fig. 9a corresponds to the bottom surface of the main surface-breaking RCF crack, presumably caused by plastic flow and ductility exhaustion [33,34] although coarse grinding during maintenance operations could have also led to ridges being folded over to form a ledge, which then acts as a crack initiation site. In Fig. 9b, distinct areas of homogeneous topographical contrast, suspected to be white-etching matter (later corroborated through TEM), can be seen running along both sides of the length of the crack. In rails, the shear stresses due to rolling contact fatigue have a maximum at the surface and at a depth of ~2 mm or deeper for decreasing friction coefficients due to an elliptical contact patch in rail/wheel contact, as opposed to a strip contact in the case of laboratory RCF tests [35]. The depth of this crack indicates a prolonged propagation stage from the surface rather than a high
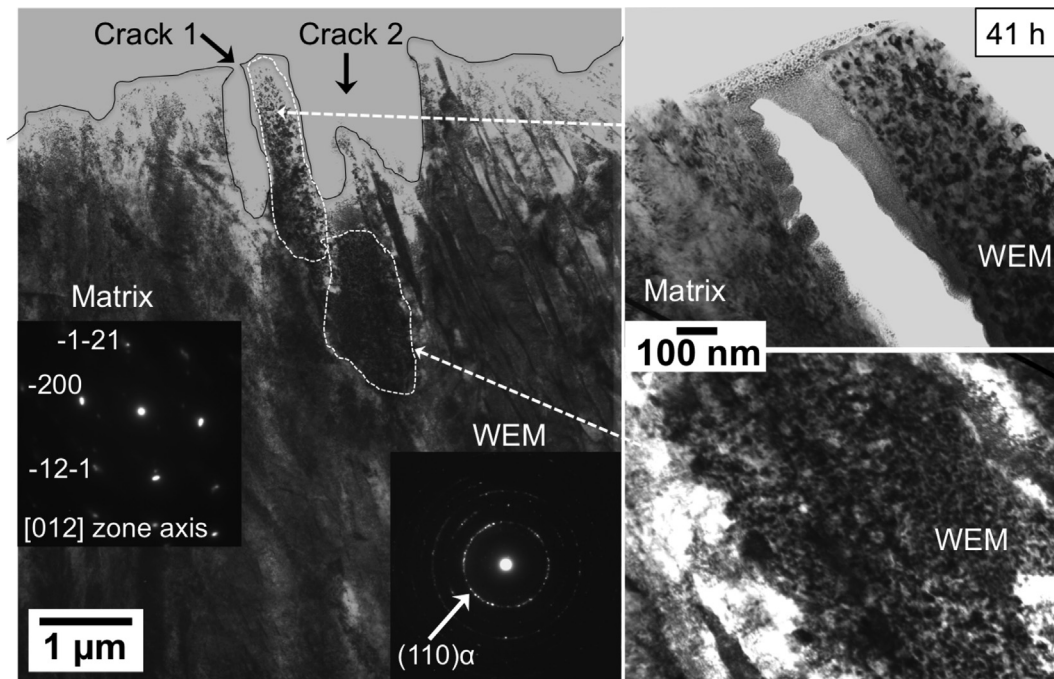

Fig. 6. Bright field TEM images of lamella FIB-1 (41 h sample) and associated selected area electron diffraction patterns.
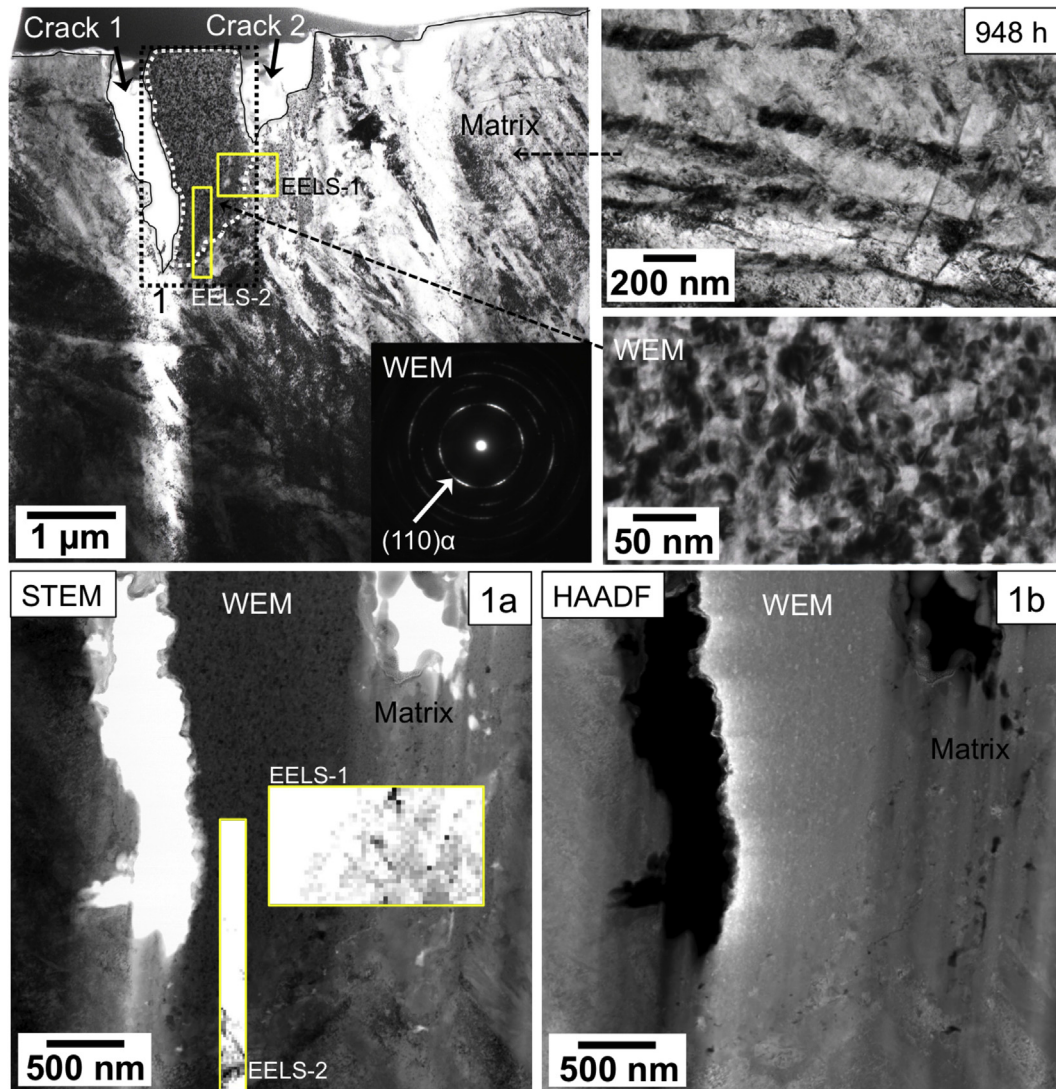
Fig. 7. Bright field TEM images of lamella FIB-2 (948 h sample) with high magnification frames of the matrix and WEM with an associated selected area electron diffraction pattern. The WEM and its vicinity are also shown using STEM in 1a for higher resolution and HAADF imaging in 1b for chemical contrast. The EELS maps marked with yellow rectangles were obtained using 200 kV, ~1000 pixels, step sizes of 17–31 nm, a pixel dwell time of 0.5 s, and filtering a K edge energy of 284 eV for carbon by adjusting the low and high-loss levels to achieve a representative contrast. (For interpretation of the references to colour in this figure legend, the reader is referred to the web version of this article.)

friction coefficient since it is a branch and not a subsurface initiated crack. The long propagation stage allowed sufficient crack face rubbing, which is manifested by the large portions of suspected WEM observed. It is also worth noting that this crack shows the same signs of ductile failure as the butterfly cracks presented previously, such as dimples and blunted tips (Fig. 9d) despite the bainitic matrix not being nanostructured, suggesting that the ductility originates from the lack of carbides in the bainite rather than the refinement of the structure.

The TEM images and electron diffraction patterns of the lamella extracted from the suspected WEM regions of the serviced rail (FIB-3) are presented in Fig. 10. As opposed to the WEM found in butterflies, which has a dotted pattern distinguishable even at low TEM magnifications, this one is much finer and can only be distinguished as such at very high magnifications and in close proximity to cracks. Otherwise, a low magnification overview of region 2 shows how this WEM has a structure reminiscent of the bainitic matrix once present before deformation.

In regions further from cracks, the WEM maintains a structured appearance even at higher magnifications including features such as twins, plate boundaries, voids, and some microcracks. Nevertheless, selected area electron diffraction patterns reveal that there is no compositional difference between the finer regions and the more structured regions further from cracks apart from some stronger individual reflexions of ferrite in the structured areas suggesting slightly less grain refinement. In any case, the ring electron diffraction patterns confirm that both regions are in fact white-etching matter as previously suspected.

These diffraction patterns are similar to the ones obtained for the white-etching butterflies in the nanostructured bainite, except that austenite persists in the WEM of the rail steel. Given the depth of the region below the contact, reaustenitisation [36–39] cannot explain the presence of the austenite, but it is possible that the austenite is mechanically stabilised by plastic deformation [40] and its small grain size [41]. The question then arises as to why the austenite was not retained in the WEM of the butterflies in the nanostructured bainite. The carbon concentration of the austenite is controlled by the T_0 curve [42] and should reach similar
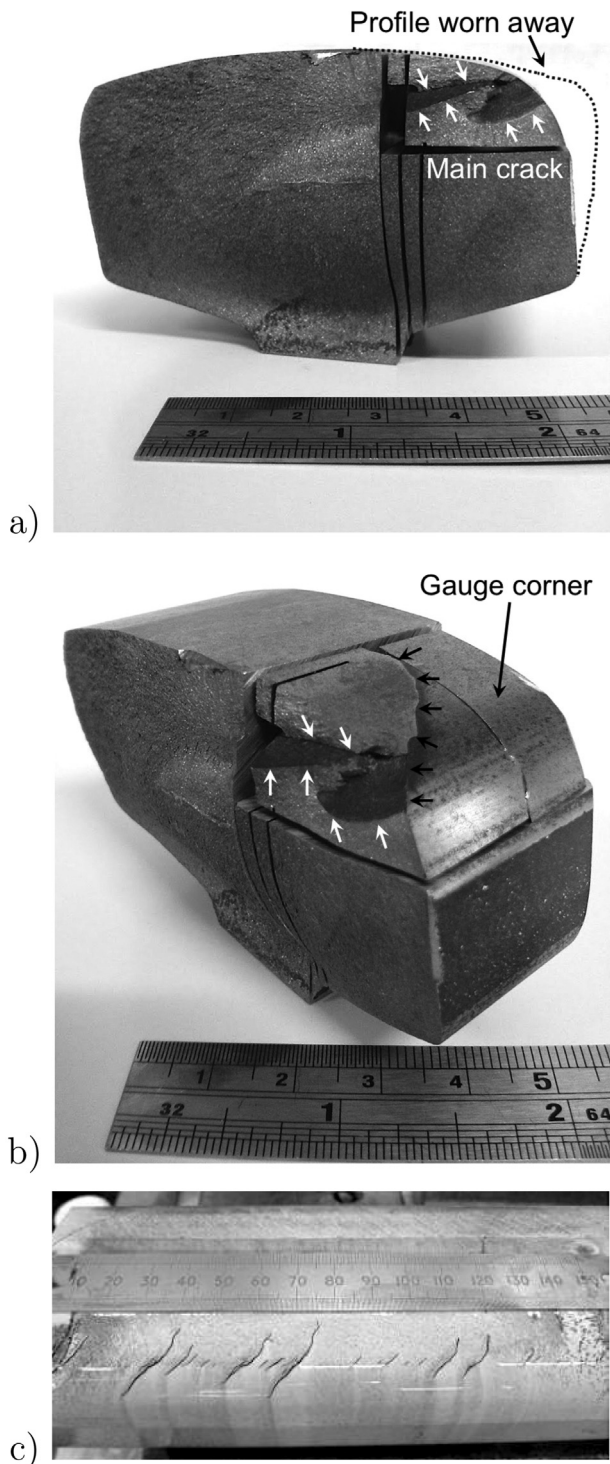
a)

b)

c)

Fig. 8. Serviced carbide-free bainitic rail showing: a) the original profile shape marked with a dotted black line and the subsurface edges of the main surface-breaking crack (white arrows), b) the gauge corner where the RCF crack breaks the surface (black arrows) and the crack edges under the surface (white arrows), and c) sample extracted from track after rust removal using fine SiC paper where the running direction is along the length of the ruler used for scale.

concentrations in both steels in spite of their large difference in average carbon concentration. One possibility is that the butterfly WEM is located in the region of maximum shear stress in the RCF test, whereas the rail WEM is located much deeper and hence should experience lower stresses. Furthermore, the rail experiences a combination of rolling and sliding, which moves the location of the maximum shear stress closer to the contact surface, e.g. Ref. [4]. It is speculated that the relative softness of the WEM in the rail can be understood in part due to its content of retained austenite and there may even be further partitioning of carbon into the austenite from the bainitic ferrite, which is known to contain excess carbon [43], facilitated by the fine structure and defect density therein.

In order to validate these ideas and understand the role of carbon redistribution in the formation of white-etching matter and its resulting hardness, chemical mapping of light elements was performed on the SEM rail sample using NanoSIMS, for the first time on white-etching matter. This technique was used instead of EELS due to the latter's dependency on sample thickness and the fact that the extracted lamella FIB-3 curled up under the electron beam due to the presence of crack networks. The NanoSIMS results from four of the most representative regions (marked in Fig. 9) are shown in Fig. 11. The number of counts vary from region to region depending on the number of planes summed together to generate the images of each site; NanoSIMS-1 (2 planes), NanoSIMS-2 (10 planes), NanoSIMS-3 (12 planes), and NanoSIMS-4 (18 planes). Carbon, detected as $^{12}C^-$ ions, can be clearly seen to enrich the retained austenite regions of the matrix, but is generally depleted from the WEM (Fig. 11-ii). In order to compare the carbon content between the matrix (as a mixture of retained austenite and bainitic ferrite) and the WEM, carbon counts per pixel were calculated for seven different areas (~10 × 10 μm) of the matrix across six of the analysed regions (50 × 50 μm), as well as for eleven areas of WEM across seven analysed regions giving a carbon matrix/WEM ratio that ranges from 1.06 to 2.72 with an average of 1.70. This means that the WEM has an average of ~40% less carbon than the matrix. When analysed at higher magnifications, small islands enriched in carbon were found within the WEM in close proximity to the matrix (Fig. 11Dii), which are suspected to be islands of retained austenite, stabilised by their excess carbon content as previously speculated.

A surprising finding in the NanoSIMS results was the relatively high signal of oxygen, measured as $^{16}O^-$ ions, in the WEM in comparison with the matrix (Fig. 11-iii). Due to the fact that the crack analysed broke the surface, it is speculated that the beating action of the crack faces incorporated oxygen and nitrogen (Fig. 11D-iv) into the WEM. It is worth mentioning that rails run without lubrication so it is unlikely the oxygen enrichment originates from lubricant breakdown. An alternative mechanism responsible for some of the carbon depletion of the WEM could be the possible formation of CO at the surface due to the ingress of oxygen into the deformed region. Although NanoSIMS could not be performed on the nanobainitic RCF samples due to the difficulty of finding small and scarce butterflies in unetched samples, it would not be expected to find oxygen incorporated into the WEM butterfly wings since butterfly cracks are subsurface initiated and normally do not break the surface. An analysis of sulphur ($^{32}S^-$) in the matrix revealed the potential presence of sulphides, most likely MnS, in the matrix (Fig. 11A-iv), although the counts obtained were too few to reach any definite conclusions. Phosphorous was expectedly found to match the path of the crack due to its embrittling effect (Fig. 11C-iv), whilst boron, despite its small concentration in this alloy, was found to decorate the prior austenite grain boundaries (Fig. 11B-iv) [44–46].
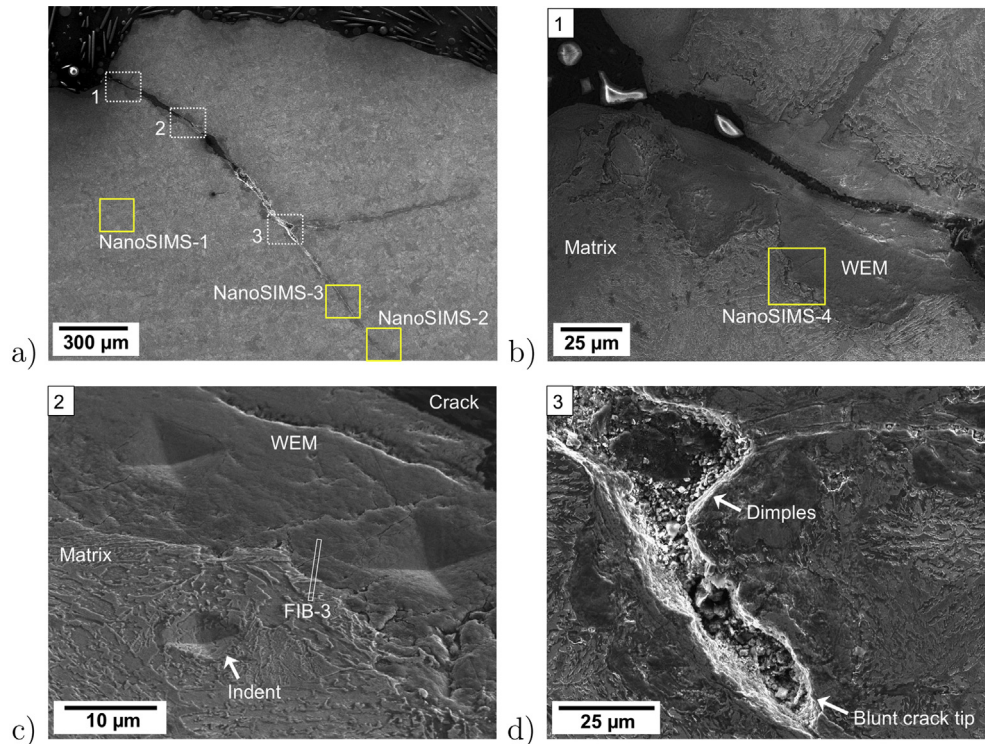
Fig. 9. Secondary electron SEM images of serviced carbide-free bainitic rail showing a) an overview of the crack, b) the crack mouth showing large areas of surrounding WEM, c) position of extracted lamella FIB-3 observed at 52° with respect to the electron beam to show also the relative difference of indent size between the WEM and matrix, and d) crack tip showing signs of ductile failure. The yellow solid line squares denote some areas analysed with NanoSIMS. (For interpretation of the references to colour in this figure legend, the reader is referred to the web version of this article.)

4. Summary

A form of white-etching matter that is *softer* than its surroundings has been found to form in the vicinity of cracks initiated at inclusions and free surfaces. Detailed characterisation using NanoSIMS and EELS has demonstrated the redistribution of light elements during localised deformation; the observed changes are consistent with the relative softness of the white-etching deformed regions.

The experimental evidence presented shows that white-etching matter can form around cracks due to the rubbing of their surfaces under cyclic stresses even when the steel does not contain carbon; the white-etching characteristic is due to the very fine scale of the structure generated. However, in the absence of prior carbides, the white-etching material is soft and hence less damaging than when carbides dissolve due to the deformation because in the latter case, the white-etching matter is harder than its surroundings. The damage potential therefore depends more on the presence or absence or carbides in the microstructure prior to service. It is clear therefore that failure mechanisms common in bearing steels can be mitigated by eliminating proeutectoid cementite that is usually present in the microstructure. It would be advantageous to focus on the development of steels that are free from such carbides. It is speculated that substitutional solutes may also affect this conclusion if they influence the stability of the proeutectoid carbides. Simultaneously, efforts to increase the ductility of such bearing and rail steels, either in attempts to lengthen the time for crack initiation or to stall crack propagation via tip blunting, must also yield positive results.

5. Conclusions

The following conclusions can be drawn for the observations presented:

- Evidence is presented for the occurrence of white-etching butterflies and white-etching cracks even in cementite-free alloys. Since white-etching matter is simply a severely deformed and mechanically mixed region, it should be a generic phenomenon irrespective of the steel concerned, although it is emphasised that its mechanical properties will depend on the detailed microstructure prior to exposure to RCF.
- White-etching butterfly wings in carbide-free nanobainite and white-etching cracks in a carbide-free bainitic rail are respectively ~10% and 48% softer than the surrounding matrix. The minor softness of the butterfly WEM is attributed to its carbon depletion as observed through EELS, whereas the major softness of the rail WEM is thought to be caused by the presence of fine retained austenite grains in the region and carbon depletion, as observed by NanoSIMS. This is in contrast to quenched and tempered martensitic steels where rolling contact fatigue leads to the dissolution of cementite creating WEM that is harder than the original matrix. Both hard and soft WEM have similar structures as confirmed by the ring-shaped electron diffraction patterns obtained.
- The butterfly cracks initiated from inclusions in the nano-structured bainite and the surface initiated rolling contact fatigue cracks in the bainitic rail show signs of ductile failure such as blunted tips, discontinuity, and dimples at the fracture
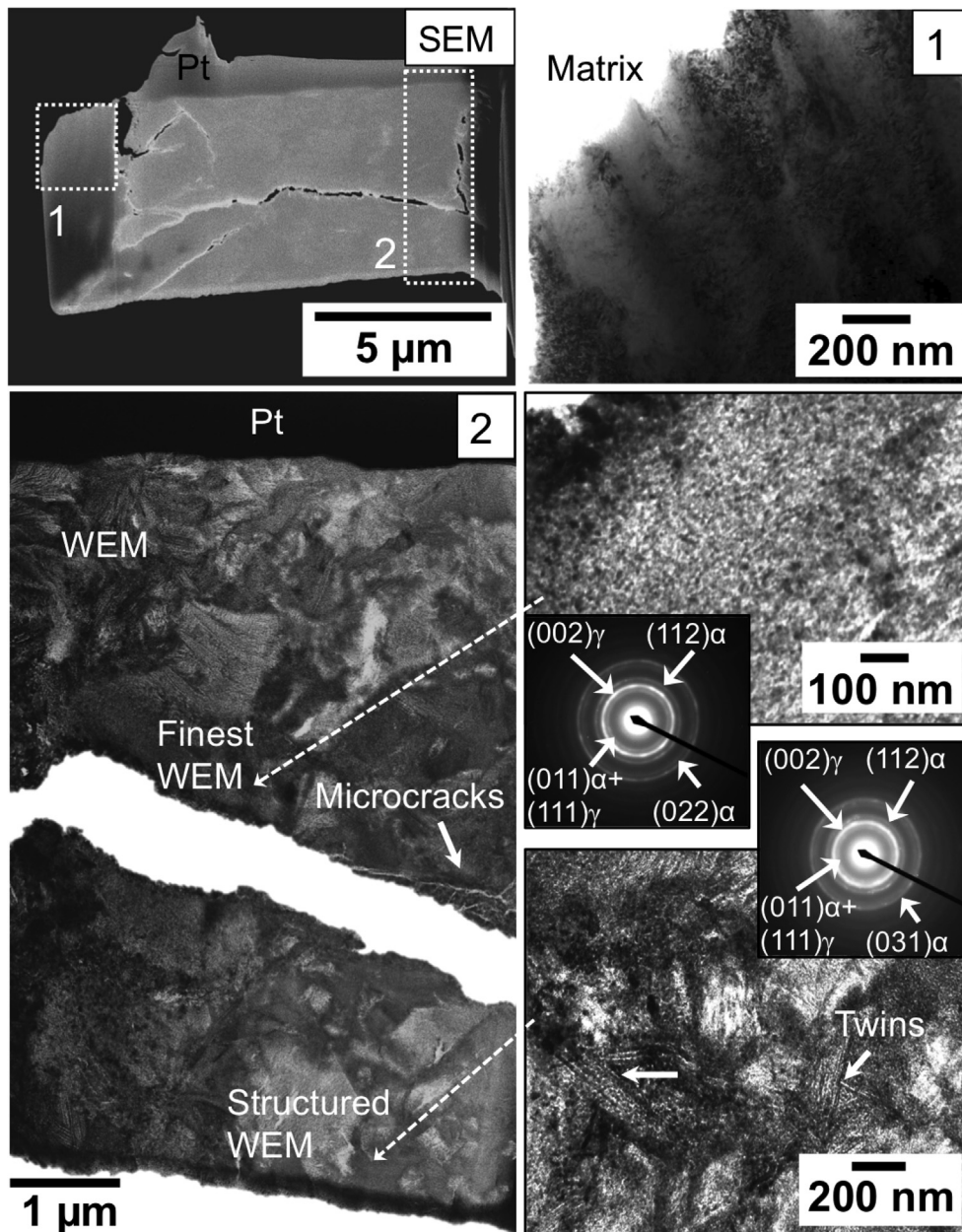
Fig. 10. Lamella FIB-3 extracted from the serviced rail as seen during the last thinning stage inside the focused ion beam SEM (secondary electron image) and bright field TEM images of the matrix in area 1 and WEM in area 2 with high magnification images and respective selected area electron diffraction patterns of regions adjacent and distant from a crack.

surfaces. This is again contrary to the brittle (butterfly) cracks present in standard martensitic steels despite tempering. Both types of cracks, ductile and brittle, show WEM formation around them even after short running periods under RCF.

- Despite the limited number of observations, the soft white-etching butterflies found in the nanostructured bainite show no crack lengthening even after 948 h of testing. Some authors have expressed the possibility of cracks initially forming hard WEM through the rubbing of their faces but once this action

dissolves the surrounding carbides and hardens the WEM, further propagation of both the crack length and white-etching area would take place concomitantly. This does not seem to occur with soft WEM, although a statistical study of butterfly crack length in carbide-free bainite would be required to reach a more categorical conclusion.

- Crystallographic maps using EBSD suggest that the nano-structure composed of carbon-enriched retained austenite is relatively stable even in the regions of highest subsurface shear
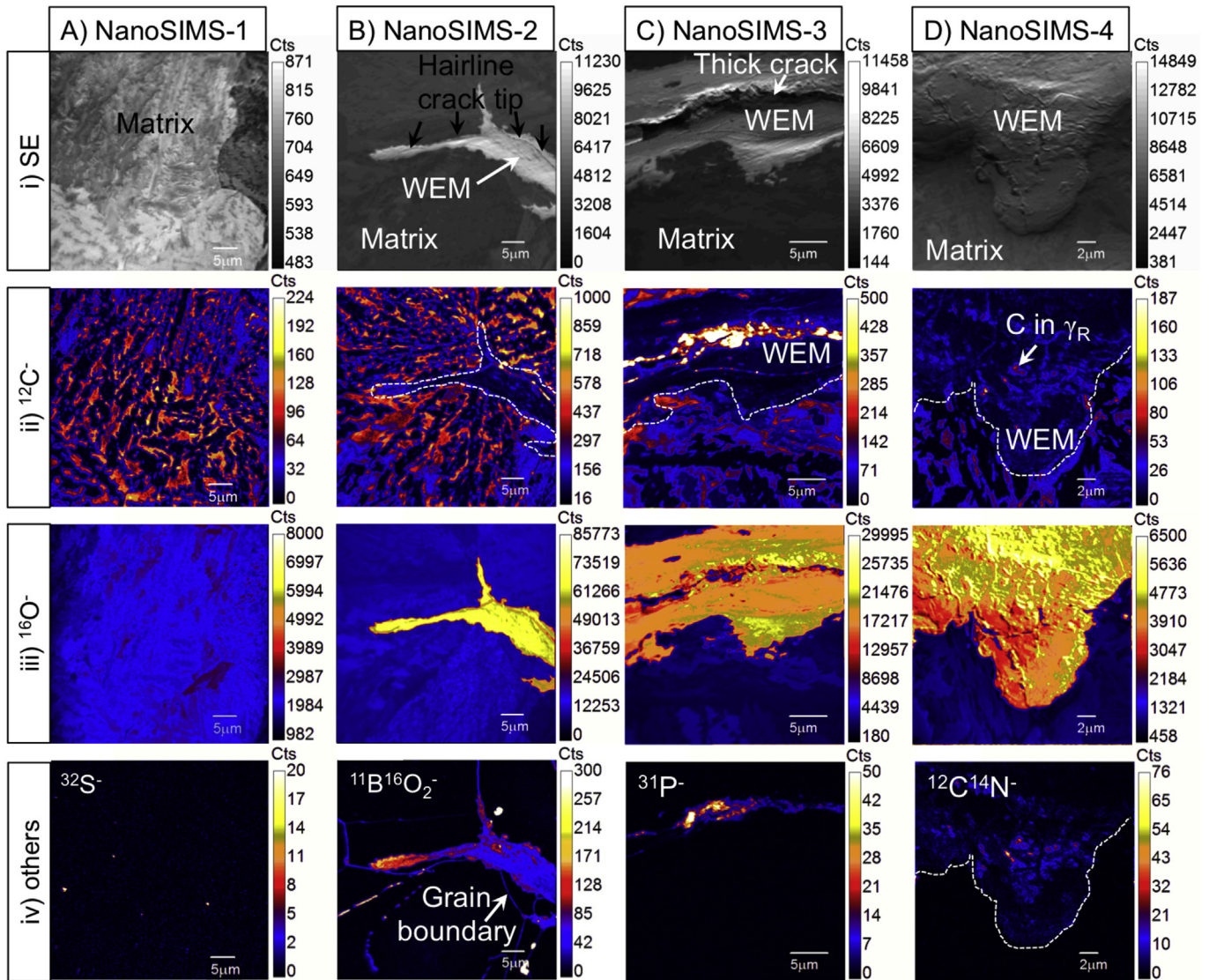
Fig. 11. NanoSIMS maps from A) the matrix (NanoSIMS-1), B) the very tip of the branched crack (NanoSIMS-2), C) a region next to a wider section of the crack (NanoSIMS-3), and D) region around the crack mouth (NanoSIMS-4), as shown in secondary electron (SE) images. Different elements such as carbon (C), oxygen (O), nitrogen (N), sulphur (S), boron (B), and phosphorous (P) were mapped as respectively indicated. Some borders between the matrix and WEM are marked with a white dashed line for clarity. (For interpretation of the references to colour in this figure legend, the reader is referred to the web version of this article.)

stresses, which is a requirement for bearing steels. Further studies to assess the dimensional and microstructural stability of this alloy under rolling contact are needed.

- EELS measurements suggest a slightly lower amount of carbon at the white-etching butterfly wings in comparison with the nanostructured bainitic matrix, which could explain their lower hardness.
- NanoSIMS measurements of the matrix and WEM in carbide-free bainite of a serviced rail reveal a significant and consistent carbon depletion of the WEM regions in comparison to the matrix average (~40% less carbon), which is partially responsible for the 48% drop in hardness compared to the matrix. This technique also evidenced oxygen enrichment of the WEM possibly due to the beating action of the crack faces whilst open to the atmosphere, boron enrichment of the prior austenite grain boundaries, and phosphorous along the crack path.
- Further studies using nanostructured bainite in actual bearings are needed to evaluate how beneficial soft white-etching matter could be in retarding white-structure flaking of gearbox

bearings against the void generation damage mechanism that this alloy displays. It would also be interesting to investigate the possibility of obtaining soft white-etching butterflies and cracks in martensitic 1C-1.5Cr bearing steel by eliminating carbides or making them more thermodynamically stable.

- Likewise, further work is needed to evaluate the implications that soft white-etching matter could have in the wear and rolling contact fatigue performance of rails, as well as determining if the white-etching layers on carbide-free rails share the same properties as the white-etching crack characterised in this study.
- Since hard white-etching matter around defects has now been shown that can also be soft in the absence of carbides, a clarification of the terms used in this subject is relevant to avoid confusion with soft white-etching bands, also depleted in carbon, that can form in the subsurface of bearings without the presence of defects such as inclusions, voids, or cracks in their immediate vicinity. Therefore, the terms suggested are: *Hard WEM* (e.g. butterfly WEM in martensitic steel), *Soft WEM* (e.g.

the WEM in butterflies and WECs from the bainitic steels presented in this paper), and *WEBs* (e.g. low and high angle soft white-etching bands).

Acknowledgements

References

[1] F.G. Caballero, H.K.D.H. Bhadeshia, K.J.A. Mawella, D.G. Jones, P. Brown, Very strong, low–temperature bainite, Mater. Sci. Technol. 18 (2002) 279–284.

[2] H.K.D.H. Bhadeshia, Nanostructured bainite, in: Proceedings of the Royal Society of London A, vol. 466, 2010, pp. 3–18.

[3] A. Leiro, Microstructure Analysis of Wear and Fatigue in High-si Austempered Steels, Ph.D. thesis, Lulea University of Technology, 2014.

[4] S.D. Bakshi, A. Leiro, B. Prakash, H.K.D.H. Bhadeshia, Dry rolling/sliding wear of nanostructured bainite, Wear 316 (2014) 70–78.

[5] T. Sourmail, V. Smanio, C. Ziegler, V. Heuer, M. Kuntz, F.G. Caballero, C. Garcia-Mateo, J. Cornide, R. Elvira, A. Leiro, E. Vuorinen, T. Teeri, Novel Nano-structured Bainitic Steel Grades to Answer the Need for High-performance Steel Components (NANOBAIN), Final report. grant agreement RFSR-CT-2008–00022, European Commission: Research Fund for Coal and Steel, 2013.

[6] W. Solano-Alvarez, E.J. Pickering, H.K.D.H. Bhadeshia, Degradation of nano-structured bainitic steel under rolling contact fatigue, Mater. Sci. Eng. A 617 (2014) 156–164.

[7] H.K.D.H. Bhadeshia, Steels for bearings, Prog. Mater. Sci. 57 (2012) 268–435.

[8] W. Solano-Alvarez, J. Duff, M.C. Smith, H.K.D.H. Bhadeshia, Elucidating white-etching matter through high strain-rate tensile testing, Mater. Sci. Technol. (2016), http://dx.doi.org/10.1080/02670836.2016.1195981.

[9] H.K.D.H. Bhadeshia, W. Solano-Alvarez, Critical assessment 13: elimination of white etching matter in bearing steels, Mater. Sci. Technol. 31 (9) (2015) 1011–1015.

[10] M.-H. Evans, White structure flaking in wind turbine gearbox bearings: effects of 'butterflies' and white etching cracks, Mater. Sci. Technol. 28 (2012) 3–22.

[11] M.H. Evans, A.D. Richardson, L. Wang, R.J.K. Wood, Serial sectioning investigation of butterfly and white etching crack (WEC) formation in wind turbine gearbox bearings, Wear 302 (1) (2013) 1573–1582.

[12] J. Gegner, Tribological Aspects of Rolling Bearing Failures in Tribology: Lubricants and Lubrication, in: Chapter 2, SKF GmbH, Department of Material Physics/Institute of Materials Science, University of Siegen, Germany, 2011.

[13] J. Gegner, W. Nierlich, Frictional Surface Crack Initiation and Corrosion Fatigue Driven Crack Growth, in: Wind Turbine Tribology Seminar, Broomfield, CO, USA, 2011.

[14] M.H. Evans, An updated review: white etching cracks (WECs) and axial cracks in wind turbine gearbox bearings, Mater. Sci. Technol. 32 (11) (2016) 1133–1169.

[15] R. Österlund, O. Vingsbo, L. Vincent, P. Guiraldenq, Butterflies in fatigued ball bearings - formation mechanisms and structure, Scand. J. Metall. 11 (1982) 23–32.

[16] A. Grabulov, R. Petrov, H.W. Zandbergen, EBSD investigation of the crack initiation and TEM/FIB analyses of the microstructural changes around the cracks formed under rolling contact fatigue, Int. J. Fatigue 32 (2010) 576–583.

[17] NPL, MTDATA, Software, National Physical Laboratory, Teddington, U.K, 2006.

[18] E. Kozeschnik, B. Buchmayr, MATCALC - a simulation tool for multicomponent thermodynamics, diffusion and phase transformations, in: H. Cerjak (Ed.), International Seminar on the Numerical Analysis of Weldability, vol. 5, Maney, London, U.K, 1999, pp. 349–361.

[19] W. Solano-Alvarez, H.K.D.H. Bhadeshia, Distinguishing cause and effect in bearing steel failure: part 2, Metall. Mater. Trans. A 45 (2014), http://dx.doi.org/10.1007/s11661–014–2431–x.

[20] C. Jeanguillaume, C. Colliex, Spectrum-image: the next step in eels digital acquisition and processing, Ultramicroscopy 28 (1–4) (1989) 252–257.

[21] R.F. Egerton, Electron Energy-loss in the Electron Microscope, third ed., Springer, 2011.

[22] P.C. Becker, Microstructural changes around non–metallic inclusions caused by rolling–contact fatigue of ball–bearing steels, Met. Technol. 8 (1981) 234–243.

[23] G. Guetard, I. Toda-Caraballo, P.E.J. Rivera-Diaz-Del-Castillo, Damage evolution around primary carbides under rolling contact fatigue in VIM-VAR M50, Int. J. Fatigue 91 (1) (2016) 59–67.

[24] M.N. Lewis, B. Tomkins, A fracture mechanics interpretation of rolling bearing fatigue, Proc. Inst. Mech. Eng. Part J-J. Eng. Tribol. 226 (5) (2012) 389–485.

[25] J.-H. Kang, Mechanisms of Microstructural Damage during Rolling Contact Fatigue of Bearing Steels, Ph.D. thesis, University of Cambridge, 2013.

[26] M.J. Peet, P. Hill, M. Rawson, S. Wood, H.K.D.H. Bhadeshia, Fatigue of extremely fine bainite, Mater. Sci. Technol. 27 (2011) 119–123.

[27] K.L. Johnson, Contact Mechanics, Cambridge University Press, Cambridge, U. K., 1985.

[28] H.K.D.H. Bhadeshia, D.V. Edmonds, Bainite in silicon steels: a new composition property approach I, Metal Sci. 17 (1983) 411–419.

[29] H.K.D.H. Bhadeshia, D.V. Edmonds, Bainite in silicon steels: a new composition property approach II, Metal Sci. 17 (1983) 420–425.

[30] A.P. Voskamp, Microstructural Changes during Rolling Contact Fatigue, Ph.D. thesis, Technical University of Delft, 1996.

[31] C. Scott, N. Guelton, Y. Ivanisenko, X. Sauvage, Applying the latest microscopy techniques to study phase transformations at rail surfaces, Rev. Metall. 103 (2006) 458–464.

[32] Rolling Contact Fatigue in Rails: a Guide to Current Understanding and Practice, Railtrack-plc, Birmingham, UK, 2001.

[33] M. Sato, P.M. Anderson, D.A. Rigney, Rolling-sliding behaviour of rail steels, Wear 162–164 (1993) 159–172.

[34] A.F. Bower, K.L. Johnson, Plastic flow and shakedown of the rail surface in repeated wheel-rail contact, Wear 144 (1991) 1–18.

[35] D.I. Fletcher, The Influence of Lubrication on the Fatigue of Pearlitic Rail Steel, Ph.D. thesis, Department of Mechanical Engineering. University of Sheffield, 1999.

[36] S.B. Newcomb, W.M. Stobbs, A transmission electron microscope study of the white etching layer on a rail head, Mater. Sci. Eng. A 66 (1984) 195–204.

[37] W. Österle, H. Rooch, A. Pyzalla, L. Wang, Investigation of white etching layers on rails by optical microscopy, electron microscopy, x-ray and synchrotron x-ray diffraction, Mater. Sci. Eng. A 303 (1) (2001) 150–157.

[38] W. Stadlbauer, W. Loos, E.A. Werner, Tribologically induced changes in the microstructure of rail surfaces, in: 2nd World Tribology Congress, vol. 651, The Austrian Tribology Society, 2001, pp. 1–4.

[39] J. Takahashi, K. Kawakami, M. Ueda, Atom probe tomography analysis of the white etching layer in a rail track surface, Acta Mater. 58 (2010) 3602–3612.

[40] S. Chatterjee, H.S. Wang, J.R. Yang, H.K.D.H. Bhadeshia, Mechanical stabilisation of austenite, Mater. Sci. Technol. 22 (2006) 641–644.

[41] H.S. Yang, H.K.D.H. Bhadeshia, Austenite grain size and the martensite-start temperature, Scr. Mater. 60 (2009) 493–495.

[42] H.K.D.H. Bhadeshia, D.V. Edmonds, The mechanism of bainite formation in steels, Acta Metall. 28 (1980) 1265–1273.

[43] H.K.D.H. Bhadeshia, Bainite in Steels: Theory and Practice, third ed., Institute of Materials, Minerals and Mining, London, U.K, 2005.

[44] J.B. Seol, N.S. Lim, B.H. Lee, L. Renaud, C.G. Park, Atom probe tomography and nano secondary ion mass spectroscopy investigation of the segregation of boron at austenite grain boundaries in 0.5 wt.% carbon steels, Metals Mater. Int. 17 (3) (2011) 413–416.

[45] N. Valle, J. Drillet, A. Pic, H.N. Migeon, Nanosims investigation of boron distribution in steels, Surf. Interface Anal. 43 (1–2) (2011) 573–575.

[46] S. Lozano-Perez, M.R. Kilburn, T. Yamada, T. Terachi, C.A. English, C.R.M. Grovenor, High-resolution imaging of complex crack chemistry in reactor steels by nanosims, J. Nucl. Mater. 374 (1) (2008) 61–68.